Maximizing Archimedes spiral packing density area

DHAIFALLAH ALMUTAIRI,[1,2,*] NAIF ALSHAMRANI,[1,2] ANDREW INGRAM,[1] ANDREW GRIECO,[1] AND YESHAIAHU FAINMAN[1]

[1]*Department of Electrical & Computer Engineering, University of California, San Diego, 9500 Gilman Dr., La Jolla, California 92093, USA.*
[2]*King Abdulaziz City for Science and Technology (KACST), P.O. Box 6086, Riyadh 11442, Saudi Arabia.*
**daalmuta@eng.ucsd.edu*

Abstract: In this paper, we experimentally demonstrate a broadband Archimedes spiral delay line with high packing density on a silicon photonic platform. This high density is achieved by optimizing the gap between the adjacent waveguides (down to sub-micron scale) in the spiral configuration. However, care must be taken to avoid evanescent coupling, the presence of which will cause the spiral to behave as a novel type of distributed spiral resonator. To this end, an analytical model of the resonance phenomenon was developed for a simple spiral. Moreover, it is demonstrated that this distributed spiral resonator effect can be minimized by ensuring that adjacent waveguides in the spiral configuration have different propagation constants (β). Experimental validations were accomplished by fabricating and testing multiple spiral waveguides with varying lengths (i.e., 0.4, 0.8, and 1.4 mm) and separation gaps (i.e., 300 and 150 nm). Finally, a Linear Density Figure of Merit (LDFM) is introduced to evaluate the packing efficiency of various spiral designs in the literature. In this work, the optimum experimental design with mitigated resonance had a length of 1.4mm and occupied an area of 60x60µm, corresponding to an LDFM of 388mm^{-1}.

1. Introduction

The Optical Delay Line (ODL) is an essential building block in numerous applications, including optical communications [1], microwave signal processing [2,3], optical gyroscopes [4], optical coherence tomography (OCT) [5], phased arrays [6], quantum computing [7], reservoir computing [8] and spectrometers [9]. Compact implementations of ODLs have been demonstrated employing several resonant designs and structures such as Bragg gratings [10], photonic crystals [11,12], coupled resonator structures [13], and stimulated Brillouin scattering photonic filters [14,15]. However, designs that use resonance phenomena to reduce the footprint of the ODL are limited in operation to discrete narrow optical frequencies in a limited spectral range. The operating bandwidth can be enhanced by cascading several resonators to increase the overall device operating bandwidth; however, the device's footprint increases commensurately [16]. Many applications, however, require true ODLs (TODL) that can work in a large optical frequency spectral band that cannot be supported with these resonance-based approaches. An alternative approach to constructing a TODL is to employ a long waveguide in a serpentine [17] or spiral [18] configuration to reduce the area footprint. In such a device, the accumulated time delay can be estimated through the following relation:$= \frac{n_g L}{c}$ Where n_g, L, and c are the group refractive index, the waveguide length, and the speed of light in a vacuum.

This manuscript proposes and demonstrates a TODL using an enhanced Archimedes spiral configuration to enable high packing density and small footprint [16,19]. Crucially, the Archimedes spiral in this work consists of clockwise and counterclockwise waveguides with differing propagation constants (β). A tapered S-shape bend waveguide to adiabatically connect these two spiral waveguides [16,19]. The mismatch minimizes the evanescent cross-coupling between adjacent waveguides and therefore allows them to be packed much more closely than in conventional designs. This approach can reduce the gap between adjacent waveguides down to the submicron scale while maintaining negligibly small evanescent coupling. Validation is performed analytically, numerically, and experimentally.

2. Design, simulation, and modeling of TODL

Theoretically, when two waveguides are placed close to each other, they become evanescently coupled, which results in crosstalk [20]. According to the coupled-mode theory, such crosstalk will be at its highest when both waveguides are designed to have identical propagation constants(β). This crosstalk can be mitigated by introducing a mismatch between the adjacent waveguide propagation constants, such that the larger the mismatch, the smaller the cross talk. This effect is significant because conventional spiral designs use adjacent waveguides with matched propagation constants, which strongly limits how close the waveguides can be packed together. The two adjacent waveguides should exhibit different propagation constants to overcome this limitation and increase the packing density. The Archimedean spiral delay line of such a structure is schematically shown in Fig. 1. The bending radius of the S-shape bend is kept as small as possible while avoiding the introduction of bending radiative loss.

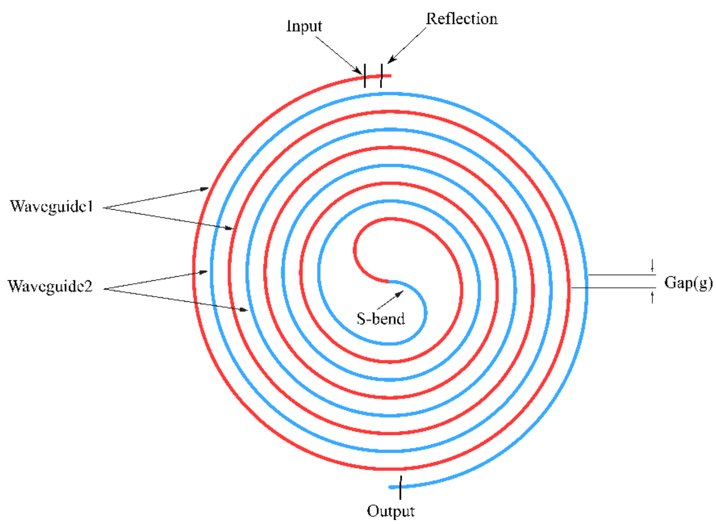

Fig.1. Schematic of the Archimedean true optical delay line (TODL) consists of two interleaved waveguides with gradually decreasing bending radiuses. As they reach the center of the spiral, those two spirals are connected in the center by an S-shape bend structure. Clockwise direction (red) is the input waveguide, and (blue) is the output waveguide, where both are separated by a gap(g).

Lumerical 2.5D variational finite-difference time-domain (varFDTD) simulations are used to investigate the effect of the width and gap of waveguides 1 and 2 on the performance of the TODL, as shown in Fig. 1. Specifically, the performance of three design cases was investigated and compared: in design (1) both waveguides were identical where the width was set to be 550 nm with a 1 µm gap, in design (2) both waveguides were identical where the width was set to be 550nm with a 300 nm gap, and in design (3) the width of waveguide 1 was 550 nm while the width of waveguide 2 was 400 nm with a 300 nm gap. Two monitors were setup in each of these simulations; one monitor was placed at the end of the spiral to measure the output transmission spectrum, denoted as output. The second monitor is located behind the input source, as seen in Fig.1, to measure the reflected spectrum back to the input, denoted as reflection. These monitors measure the reflected and transmitted spectrum that results from signal propagating through the optical delay line (TODL). The reflected spectrum is an indication of the strength of the interaction between the adjacent waveguides in the spiral delay line. This interaction causes some transmitted spectrum to propagate back to the input direction. Typically, a smaller reflected spectrum results from minimal interaction between the waveguides in the TODL. Furthermore, a larger reflected spectrum is caused by high interaction between the waveguides as the mode propagates through the spiral.

We expect to see a very low to non-existing reflected transmission spectrum from the design simulation (1) due to a large separation gap of 1μm, which is the typical separation gap used for TODL in literature [16,19]. In the design simulation (2), the reflected spectrum is due to a sub-micron gap and has no geometric dispersion since waveguides 1 and 2 have the exact dimensions. However, the effect of bending dispersion can cause variation in the propagation constant (β) and thus might reduce the total reflected spectrum. Finally, the design simulation (3) has both geometry dispersion and bending dispersion, which offers a unique opportunity to observe both the effect on the propagation constant (β) and reflected mode strength.

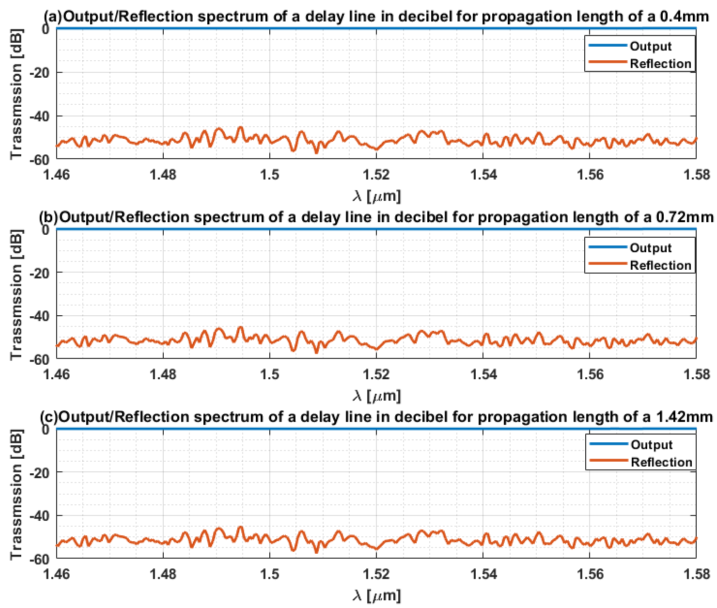

Fig. 2. Transmission spectrums of the simulated Archimedes spiral delay line for different propagation lengths where waveguides 1 and 2 are identical (i.e., width = 550 nm) and the gap between them is 1 μm. The blue indicates the transmitted spectrum through the suggested spiral, while the orange indicates the reflected spectrum back to the source. (a) Transmission spectrum of a delay line in decibel for propagation length of 0.4 mm. (b) Transmission spectrum of a delay line in decibel for propagation length of 0.72 mm. (c) Transmission spectrum of a delay line in decibel for propagation length of a 1.42 mm.

Fig. 2 shows the simulation of design (1), where waveguides 1 and 2 have a similar width of 550 nm and a separating gap of 1 μm. The figure shows the results of transmission and reflection spectrums of an Archimedes delay line in the spectral band of 1.46-1.58 μm when its adjacent waveguides are identical (i.e., 550 nm) with a 1 μm gap for a total length of 0.4, 0.72, and 1.42 mm as shown in Figs 2 (a-c). The results in Fig. 2 show the transmitted spectrum in decibel to be 0 dB while the reflected signal is maintained at less than -40 dB for all propagation lengths of 0.4, 0.72, and 1.42 mm. It can be concluded that, as expected, there is no interaction between the adjacent waveguide in the Archimedes spiral. Also, the reflected spectrum does not vary as a function of propagation length which confirms that there is no coupling in this Archimedes spiral TODL. It is important to note that even though the waveguides have the same width, they experience different propagation constant (β) due to the bending dispersion due to the low bending radius [21]. This effect is not visible here due to the large separation gap in this design; however, this dispersion effect is observed in Fig.3 and Fig.4.

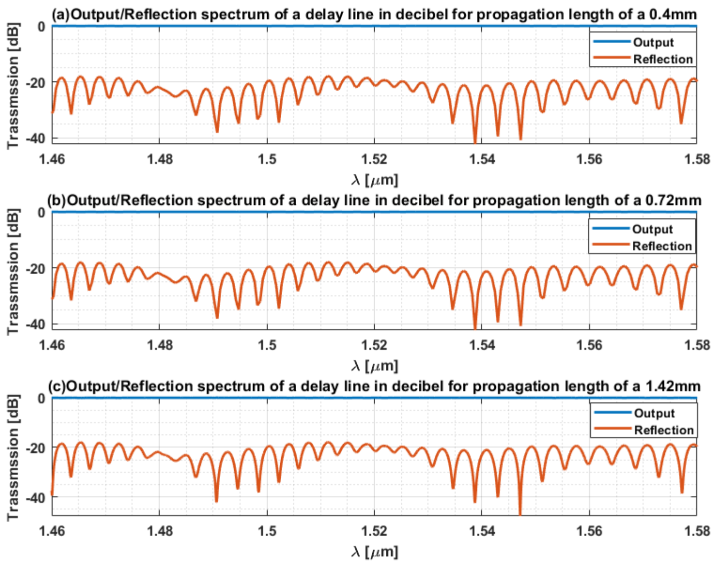

Fig. 3. Transmission spectrum of the simulated Archimedes spiral delay line with different propagation lengths where both waveguide widths are identical (i.e., width = 550 nm) and the gap between them is 300 nm. The blue indicates the transmitted spectrum through the suggested spiral, while the orange indicates the reflected spectrum back to the source. (a) Transmission spectrum of a delay line in decibel for propagation length of 0.4mm. (b) Transmission spectrum of a delay line in decibel for propagation length of 0.72mm. (c) Transmission spectrum of a delay line in decibel for propagation length of 1.42mm.

Fig. 3 shows the simulation of design (2), where waveguides 1 and 2 have similar widths of 550 nm with a separating gap of 300 nm. An oscillation of less than 0.1% is observed in the transmitted spectrum for all propagation lengths of 0.4, 0.72, and 1.42 mm (see Fig.3(a-c)). A comparison of the results of simulated design (1) in Fig. 2 and simulated design (2) in Fig. 3 shows that the reflected spectrum increases from approximately -40dB to -20dB when the gap is decreased from 1 um to 300nm. The reflected spectrum does not vary as a function of the length of the delay line, which shows that the transmission spectrum is not significantly affected by any resonant phenomenon caused by the interaction between the adjacent waveguides under a small separation gap. If such resonance were to occur, there would be a clear dependence of the reflected spectra on the spiral length (because each length would have a different resonant cavity length). Instead, the signal-to-noise ratio increase is more likely a result of imperfect simulation meshing of the curved waveguide. The result indicates a negligibly small interaction between the two adjacent waveguides. Although this design is not affected by geometry dispersion, it is effect by the bending dispersion, which causes a different propagation constant(β) for each waveguide; such a difference in the propagation constant limits the interaction in the spiral.

Fig. 4 shows the simulation of design (3), where the width of waveguide 1 was 550 nm while the width of waveguide 2 was 400 nm with a 300 nm gap. For the delay line of 0.4 mm length, we observe an approximate 5% oscillation in the transmission spectrum (see Fig.4(a)), significantly increasing across the spectrum for the delay lengths of 0.72mm (see Fig. 4(b)) and 1.42mm (see Fig.4(c)). This oscillatory behavior can be characterized as a result of the formation of a distributed spiral resonator due to coupling between adjacent waveguides, where its cavity length varies with the total length of the spiral optical delay line. With this hypothesis, the Free Spectral Range (FSR) for the 0.72 mm and 1.42 mm long spirals in Fig.4(b) and Fig. 4(c) is approximately 66.7 nm and 50nm, respectively. The corresponding Q factors for these resonators are estimated to be 38.8 and 50 for spiral lengths of 0.72 and 1.42 mm, respectively.

When comparing Fig. 3(b) and Fig. 4(b), we observe that when the adjacent waveguides are identical (Δw=0), the reflected signal is at -20 dB, while when Δw=150 nm, the reflected signal oscillates between -10 to 0 dB. We can conclude that in this design, a resonance effect is caused by coupling between the adjacent waveguides. This coupling is enhanced by the combined effect of the geometry and bending dispersion. However, the observed resonator needed to be analyzed further to understand it.

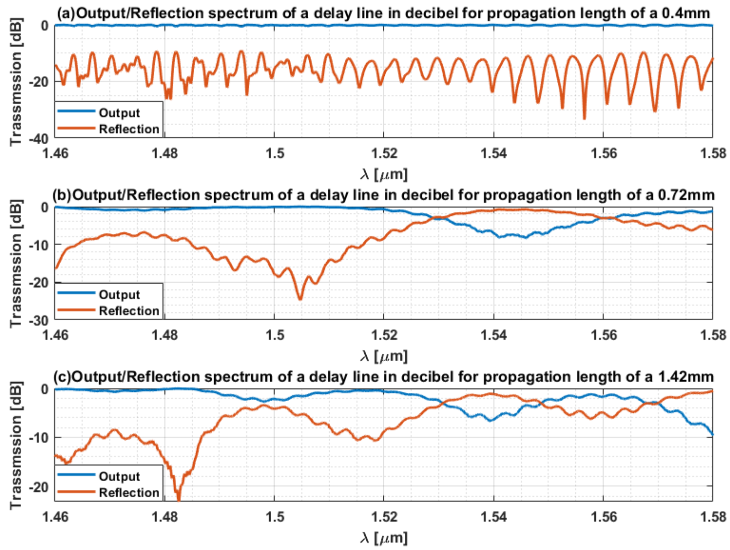

Fig. 4. Transmission spectrum of the simulated Archimedes spiral delay line with different propagation lengths where waveguide 1 and 2 widths are 550 and 400nm, respectively, and the gap between them is 300 nm. The blue indicates the transmitted spectrum through the suggested spiral, while the orange indicates the reflected spectrum back to the source. (a) Transmission spectrum of a delay line in decibel for propagation length of 0.4mm. (b) Transmission spectrum of a delay line in decibel for propagation length of 0.72mm. (c) Transmission spectrum of a delay line in decibel for propagation length of 1.42mm.

3. Analysis of the resonant behavior in the Archimedes TODL

We next discuss a simplified analytical model to describe the resonant transmission and reflection of a closely packed Archimedes spiral TODL. When formulating the problem mathematically, it is tempting to try the matrix approach that would solve the problem in terms of supermodels. However, this approach runs into problems due to the spatial variation of the coupling coefficient along the spiral length.

Consequently, it is desirable to use a more flexible approach that uses reflection coefficients to represent the coupling regions in the spiral. The repetitive structure of the spiral lends well to this analysis approach.

As an initial approach, we consider a simplified spiral version, as seen in Fig.5, Where the coupling is limited to a small section of each arm in the S-shape bend. The field coupling coefficients k and c for the clockwise and counterclockwise propagation with the subscripts indicating the coupling direction.

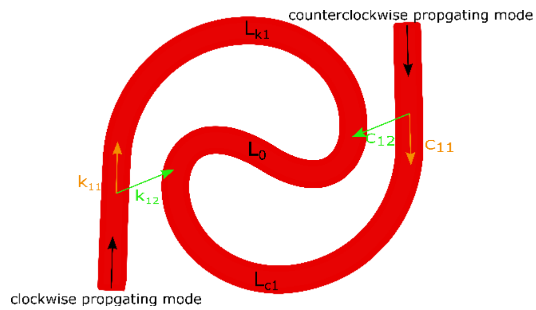

Fig. 5. Simplified coupling model in a resonator formed by a single loop spiral.

Consider the transmission coefficient as a summation similar to Airy's formulas (multiple resonant paths) illustrated in Fig. 6 for the Fabry–Pérot resonator:

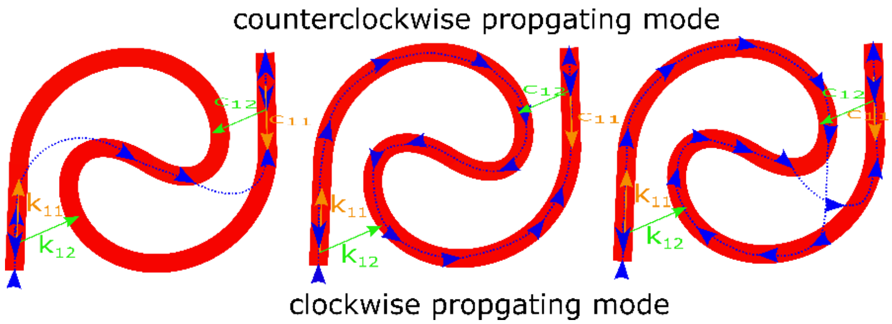

Fig. 6. The possible path the propagated mode can take.

$$
\begin{aligned}
t_s = {} & \underbrace{k_{12}\exp(i\beta L_0)c_{12}}_{nonrepeating} \\
& + \underbrace{k_{12}\exp(i\beta L_0)c_{11}\exp(i\beta L_{k1})k_{12}\exp(i\beta L_{c1})}_{beginning\,1}\ \underbrace{c_{11}}_{ending\,1} \\
& + \underbrace{k_{11}\exp(i\beta L_{k1})c_{11}\exp(i\beta L_0)k_{11}\exp(i\beta L_{c1})}_{beginning\,2}\ \underbrace{c_{11}}_{ending\,1} \\
& + \underbrace{k_{11}\exp(i\beta L_{k1})c_{12}\exp(i\beta L_{c1})}_{beginning\,3}\ \underbrace{k_{11}\exp(i\beta L_0)c_{12}}_{ending\,2} \\
& + \underbrace{k_{12}\exp(i\beta L_0)c_{11}\exp(i\beta L_{k1})k_{12}\exp(i\beta L_{c1})}_{beginning\,1}\ \underbrace{c_{12}\exp(i\beta L_{k1})k_{12}\exp(i\beta L_{c1})}_{middle\,1}\ \underbrace{c_{11}}_{ending\,1} \\
& + \underbrace{k_{11}\exp(i\beta L_{k1})c_{11}\exp(i\beta L_0)k_{11}\exp(i\beta L_{c1})}_{beginning\,2}\ \underbrace{c_{12}\exp(i\beta L_{k1})k_{12}\exp(i\beta L_{c1})}_{middle\,1}\ \underbrace{c_{11}}_{ending\,1} \\
& + \underbrace{k_{11}\exp(i\beta L_{k1})c_{12}\exp(i\beta L_{c1})}_{beginning\,3}\ \underbrace{k_{12}\exp(i\beta L_{k1})c_{12}\exp(i\beta L_{c1})}_{middle\,1}\ \underbrace{k_{11}\exp(i\beta L_0)c_{12}}_{ending\,2} \\
& + \ldots
\end{aligned}
$$

Although the terms of the summation in the simplest spiral are much more complex than those in a Fabry–Pérot cavity [22], they simplify similarly. Reduce the above terms using a geometric series as follows:

$$\sum_{k=0}^{\infty} ar^k = \frac{a}{1-r}, r < 1$$

$$t_S = k_{12}\exp(i\beta L_0)c_{12} + \left(k_{12}c_{11}k_{12}c_{11} + k_{11}c_{11}k_{11}c_{11} + k_{11}c_{12}k_{11}c_{12}\right)\frac{\exp(i\beta L_0)\exp(i\beta L_{k1})\exp(i\beta L_{c1})}{1 - c_{12}\exp(i\beta L_{k1})k_{12}\exp(i\beta L_{c1})}$$

Moreover, the reflection coefficient can be written as:

$$r_S = \left[1 + k_{11}^2\exp(i\beta L_{c1})\exp(i\beta L_{k1})\right]\frac{2k_{11}k_{12}c_{11}\exp(i\beta L_0)\exp(i\beta L_{k1})}{1 - k_{12}\exp(i\beta L_{c1})c_{12}\exp(i\beta L_{k1})}$$

These expressions are similar to the Fabry–Pérot reflection coefficient equation. The leading constant terms make analytical evaluation difficult; however, they can be calculated numerically. For the simplest case of the Archimedes delay line illustrated in Fig. 5, we estimate 47.5,24.8, and 47.5µm corresponding to Lc1, L0, and Lk1's cavity lengths, respectively. To further simply the equation above, the two coupling terms k_{11} and c_{11} can be related thus:

$$c_{11} = 1 - k_{11}$$

In addition, assuming that the two sides of the simplified version of the distributed spiral resonator are similar, it is safe to assume that c_{11}=c_{12} and k_{11}=k_{12}. With these values, it is possible to plot the analytic solution from the transmitted spectrum of the equation above as a function of the coupling coefficient k_{11}, shown in Fig.7.

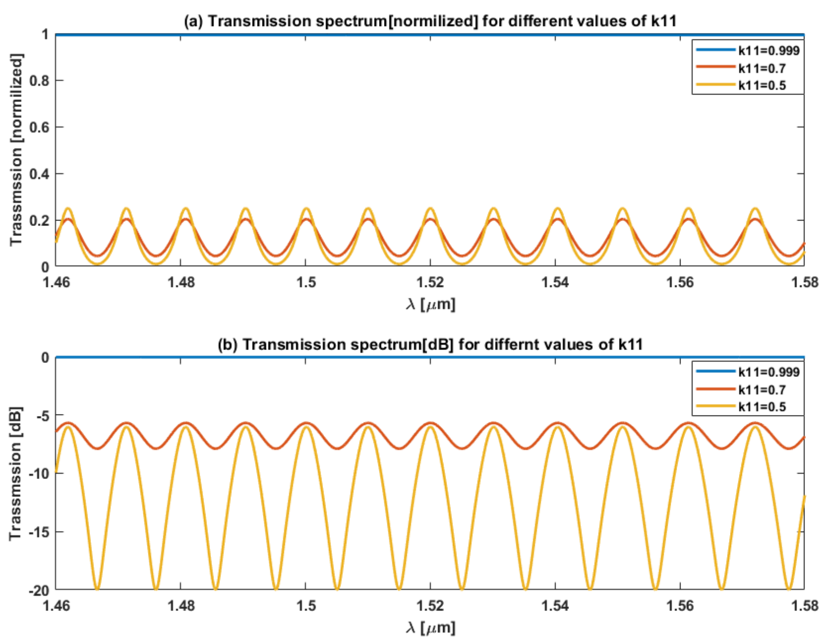

Fig. 7. Transmission spectrum as a function of cross coupling parameter k_{11} for ideal resonator loop where $|r|^2 + |t|^2 = 1$. (a) normalized transmission spectrum for k_{11} [blue=0.999, red=0.7, yellow=0.5]. (b) Transmission spectrum in decibel for k_{11} [blue=0.999, red=0.7, yellow=0.5]

Fig. 7 (a[blue line]) shows the transmission spectrum of the suggested model, in which the coupling coefficient (k_{11}) is equal to 0.999. The same resonance is observed in the transmission spectrum in Fig. 2. Fig. 7(a[red line]) shows the effect of the distributed Fabry–Pérot-like resonator when the coupling coefficient k_{11}= 0.7, which has an FWHM equal to 3.2 nm corresponding to a Q factor of 458.3. Moreover, Fig.7 (a[yellow line]) shows the same effect when the coupling coefficient k_{11}=0.5, which has an FWHM equal to 5.8 nm corresponding to a Q factor of 252. By changing the coupling coefficient (k_{11}), the effect of the distributed spiral resonator Q factor can be reduced. For this manuscript, the Fabry–Pérot-like resonator effect is undesirable and can be reduced by limiting the cross-coupling coefficient. Conversely, for other applications, a distributed spiral resonator might be helpful. In such a case, the primary way this can be achieved, as seen from the simulations in Fig.6 and Fig.5, is not to introduce a variation between the propagation constants of the two adjacent waveguides.

Strictly speaking, the above process could be used to analyze a spiral with multiple turns. However, the sheer number of new closed-loop paths introduced by each additional turn makes this quickly become resistant to analysis. However, the model is still helpful as it provides enough information that we can develop the intuition that these additional path loops will behave additively in the same way as the loops in the simple model. Therefore, we know how the spiral will behave in a general sense (there will be distinct resonance peaks) even if it is difficult to predict the exact spacing in practice accurately.

4. Fabrication and characterization

The Archimedes spiral TODL design was fabricated as part of a multi-project-wafer (MPW) run at the Applied Nanotools (ANT) foundry. The MPW run utilizes standard silicon on insulator (SOI) wafer, which consists of a 220 nm device layer and a 2 µm bottom oxide layer (BOX). The standard process of the MPW run starts with writing the design pattern on e-beam resist using electron beam lithography (EBL). Inductively Coupled Plasma Etching (ICP-RIE) is employed to transfer the pattern from the E-beam resist into the silicon layer. The sample is cladded with a 2.2 µm SiO_2 layer through Plasma Enhanced Chemical Vapor Deposition (PECVD). The overall design consists of multiple Archimedes spirals with different gaps, widths, and several spirals to demonstrate the simulation results, as seen in Fig.8.

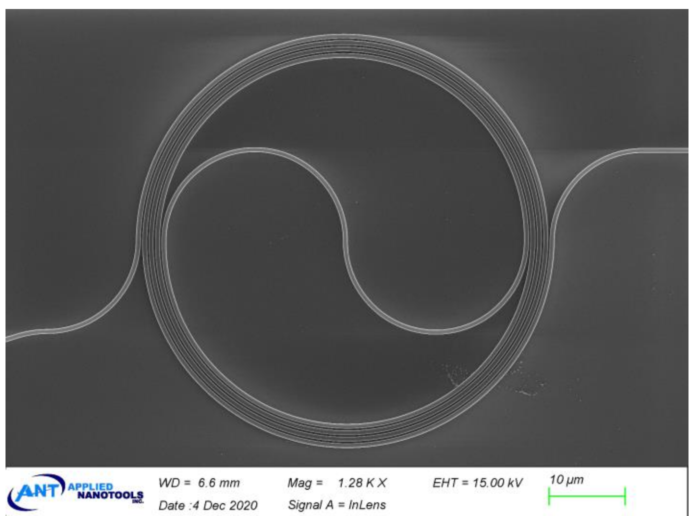

Fig.8. The SEM images of the fabricated Archimedes spiral delay lines: (a) The input and the output waveguides have similar dimensions of 550nm width, 220nm height, and a separation gap of 300nm with a total length of 0.72mm.

The device was characterized using the standard fiber-to-free space setup described previously in [23,24]. Finally, the propagation loss of the fabricated Archimedes spiral delay line is specified to be 3.8 dB/cm [25,26].

5. Results

The fabricated Archimedes spiral of the delay line is designed to observe the effect of introducing a width difference (Δw) of 0, 100, or 150 nm for the cases of a separation gap of 300nm and 150nm in Fig.9.

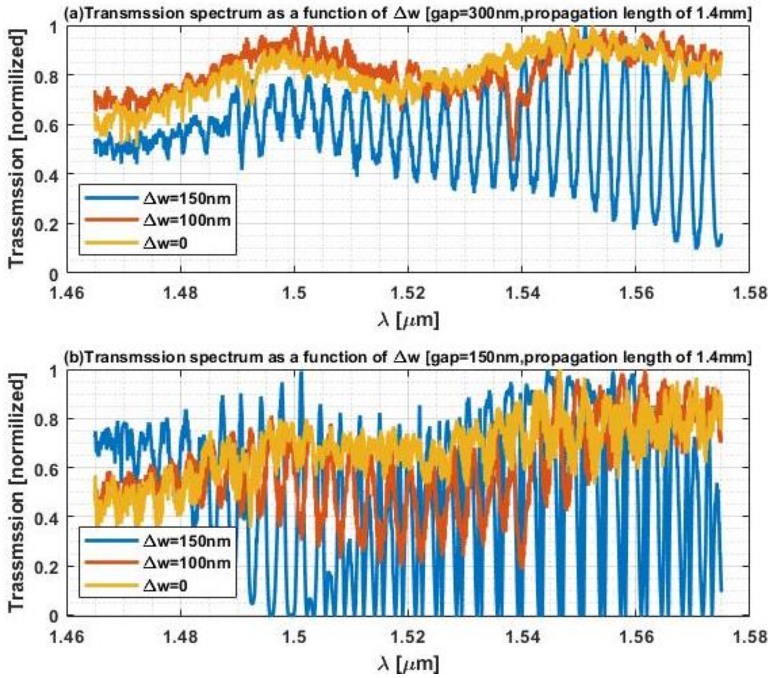

Fig.9. Measured transmission spectrum of the fabricated Archimedes spiral delay line with three different Δw at a total length of 1.4mm. The blue color indicates a difference between the adjacent waveguide (Δw) equals 150 nm. The Red color indicates a difference between the adjacent waveguide is (Δw) equal to 100 nm; the yellow color shows the difference between the adjacent waveguide is (Δw) zero. (a) measured transmission spectrum of the fabricated delay line propagation length equal to 1.4mm and separation gap equal to 300nm. (b) measured transmission spectrum of the fabricated delay line propagation length equal to 1.4mm and separation gap equal to 150nm.

Fig.9(a) shows the waveguide width difference (Δw) effect on the transmission spectrum at a gap of 300 nm and spiral length of 1.4 mm. In the transmission spectrum, when Δw=0 nm, no resonance exists in the range from 1460 nm to 1540 nm; a slight variation can be noticed from above the wavelength of 1540 nm with a variation of less than 10%. Thus, we can conclude that bending dispersion minimizes a distributed spiral resonator effect. In addition, the transmission spectrum variation percentage when Δw=0 and 100 nm is less than 9% and 20%, respectively.

However, when Δw=150 nm, the transmitted spectrum varies from 30% for wavelengths between 1460 nm to 1480 nm, to 40%, for wavelengths between 1500nm to 1540nm, in which the maximum transmission spectrum variation is shown to be 78% for wavelengths between 1560nm to 1580nm. The transmission spectrum variation shows a clear wavelength dependence, resulting from geometry dispersion-compensating for the variation in propagation constant (β) caused by bending dispersion. This effect increases the strength of coupling between the adjacent waveguides in the spirals and thus enhancing the distributed spiral resonator. The same enhancement is noticeable when Δw=100 nm, the average transmission variation is less than 20%, and the maximum variation in the transmission spectrum is 35%.

Fig.9(b) shows the transmission spectrum of an Archimedes delay line with a separation gap equal to 150 nm. At this gap, the effect of the distributed spiral resonator can be observed in all different Δw values. When Δw=150nm, the transmission varies from 40% between 1460 and 1480 nm to 84% for wavelengths between 1500 and 1540 nm. Moreover, the transmission variation is 87% for wavelengths between 1560 to 1580 nm. The same effect is noticeable when Δw=100nm with a minor transmission variation compared to when Δw=150nm. As described in the literature, coupling between waveguides is a function of the separation gap [20], hence the increased cross-coupling from the change gap from 300 to 150 nm. Furthermore, the coupling coefficient's wavelength dependence is a clear indication that the coupling which causes the distributed spiral resonator is enhanced by the smaller gap, especially when comparing these results to Fig.10(a). The presence of high resonance effects suggests that the gap of 150nm cannot be used for a typical delay line due to the high effect of the distributed spiral resonator.

It is important to note that the reflected spectrum is not measured due to the limitation of the current fiber-to-free space setup and the fabricated sample. In the future, a sample can be fabricated to include a Y-splitter at the input to extract the reflected spectrum easily.

6. Discussion

In this work, we showed a new approach to maximizing the packing density of TODL by reducing the separation gap to submicron and maintaining a minimum bending radius while also avoiding inducing radial loss. As observed in the simulation, these conditions give rise to a novel type of distributed spiral resonator. This resonator effect can be mitigated by introducing enough variation in the preparation constant (β) between the adjacent waveguides.

While the bending radius is maintained to be small enough, the two adjacent waveguides are kept in the exact dimensions to minimize coupling and thus eliminate the effect of the distributed spiral resonator. Moreover, the variation caused by the propagation constant (β) will become negligible in the case of a large enough bending radius. In that case, it would be necessary to vary the cross-section of adjacent waveguides to achieve geometry dispersion, thus introducing a mismatch in the propagation constant (β).

The presented results validate the suggested theoretical model and simulated results in Fig.3 and Fig.4. The effect of the distributed spiral resonator can be enhanced when the two waveguides have similar propagation constants, as in the case of Fig.10 when Δw=150 nm. Additionally, the effect of the distributed spiral resonator can be reduced when the waveguides have different propagation constants, as in the case of Fig.10 when Δw=0.

The fabricated design in the manuscript is compared to some of the delay line structures found in the literature (see Table1). The last column in Table 1 shows a new figure of merit called Linear Density Figure of Merit (LDFM), which evaluates the packing efficiency of various delay line design approaches.

Table 1. Comparison of various optical delay lines from literature and the fabricated design

Paper	Loss	Time delay(τ)	Approach	Bandwidth	Material	LDFM (km^{-1})
Bykhovsky [27]	0.5 dB	17.2ns	Cascaded spiral	80nm	Si_3N_4	146
Yan Li [28]	1.908 dB/cm	2.804ns	Archimedes spiral	NA	SOI	197.9
Chen [29]	0.1 dB/m	NA	Whispering gallery delay lines	NA	Si/ SiO_2	77.56
Yurtsever [30]	<0.14 dB/cm	NA	Mach-Zehnder interferometer	100nm	Si_3N_4/SiO_2	0.575
Stopinski [31]	10 dB	250 ps	Archimedes spiral	30 GHz	InP	52.632
This work	3.8 dB/cm	19.41 ps	Archimedes spiral	100nm	SOI	388

LDFM is an excellent method to evaluate the cost-effectiveness of any TODL since it occupies a large area of the chip to achieve a long delay time (τ). A more significant LDFM number indicates a higher packing density and thus a more cost-effective method to achieve the required delay time. This aspect of delay line design is often overlooked but very important to classify because the available space for integrated devices is often minimal. Finally, The proposed design in this paper shows the highest LDFM with a value of 388 km^{-1}, which is at least two times higher than the designs reported in recently published papers, as seen in Table1. The loss of the fabricated TODL is 3.8 dB/cm, which can improve by choosing a wider waveguide or changing to material that exhibits lower loss (for example, Si_3N_4), as demonstrated in Bykhovsky's work [27].

7. Conclusion:

In conclusion, we have designed, fabricated, and characterized a broadband Archimedes spiral delay line with a high packing density. The higher packing density is achieved by reducing the gap between two adjacent waveguides in the sub-micron range and maintaining a low bending radius. Waveguides with such slight separation typically experience substantial coupling-induced crosstalk that limits the device's spectral response. It was experimentally demonstrated that this effect could be mitigated by engineering the waveguides in different arms of the spiral to have different propagation constants. Furthermore, to validate this design approach, we developed an analytical model of the spiral that explicitly incorporates the evanescent coupling. This model shows that when the coupling is non-negligible, the device functions as a novel type of distributed spiral resonator. It was concluded that while maintaining a low bending radius, each waveguide experiences a different propagation constant due to the bending dispersion; thus, maintaining similar geometry for the waveguide in the spiral would limit the distributed spiral resonator effect. Finally, an LDFM is defined to evaluate the packing efficiency and cost-effectiveness of future delay line design approaches.

Funding. Defense Advanced Research Projects Agency (DSO NAC Programs); Office of Naval Research; National Science Foundation (ECCS-180789, NSF ECCS-190184, NSF ECCS-2023730); Army Research Office; San Diego Nanotechnology Infrastructure (SDNI) supported by the NSF National Nanotechnology Coordinated Infrastructure (ECCS-2025752); Quantum Materials for Energy Efficient Neuromorphic Computing-an Energy Frontier Research Center funded by the U.S. Department of Energy (DOE) Office of Science; Basic Energy Sciences (DE-SC0019273); LEED: A Lightwave Energy-Efficient Datacenter funded by the Advanced Research Projects Agency-Energy; Cymer Corporation.

Acknowledgments. Dhaifallah Almutairi and Naif Alshamrani would like to thank King Abdulaziz City for Science and Technology (KACST) for their support during their study.

Disclosures. The authors declare no conflicts of interest.

Data availability. Data underlying the results presented in this paper are not publicly available at this time but may be obtained from the authors upon reasonable request.

Reference:

1. R. W. Boyd, D. J. Gauthier, and A. L. Gaeta, "Applications of slow light in telecommunications," Opt. Photonics News 17, 18–23 (2006)
2. A. E. Willner, B. Zhang, L. Zhang, L. Yan, and I. Fazal, "Optical signal processing using tunable delay elements based on slow light," IEEE J. Sel. Top. QuantumElectron. 14, 691–705 (2008).
3. J. Capmany, B. Ortega, and D. Pastor, "A tutorial on microwave photonic filters," J. Lightwave Technol. 24, 201–229 (2006).
4. C. Ciminelli, C. E. Campanella, F. Dell'Olio, M. N. Armenise, E. Armandillo, and I. McKenzie, "Study of photonic resonant angular velocity sensors as alternativegyro technology," Proc. SPIE 10564, 105641M (2017).
5. G. Yurtsever, B. Považay, A. Alex, B. Zabihian, W. Drexler, and R. Baets, "Photonic integrated Mach-Zehnder interferometer with an on-chip reference arm for optical coherence tomography," Biomed. Opt. Express 5, 1050 (2014).
6. E. N. Toughlian and H. Zmuda, "A photonic variable RF delay line for phased array antennas," in Journal of Lightwave Technology, vol. 8, no. 12, pp. 1824-1828, Dec. 1990, doi: 10.1109/50.62877.

7. Lvovsky, A., Sanders, B. &Tittel, W. Optical quantum memory. Nature Photon 3, 706–714 (2009). https://doi.org/10.1038/nphoton.2009.231.
8. Vandoorne, K., Mechet, P., Van Vaerenbergh, T. et al. Experimental demonstration of reservoir computing on a silicon photonics chip. Nat Commun 5, 3541 (2014). https://doi.org/10.1038/ncomms4541.
9. Jahn, D., Lippert, S., Bisi, M. et al. On the Influence of Delay Line Uncertainty in THz Time-Domain Spectroscopy. J Infrared MilliTerahz Waves 37, 605–613 (2016). https://doi.org/10.1007/s10762-016-0250-4.
10. I. Giuntoni, D. Stolarek, D. I. Kroushkov, J. Bruns, L. Zimmermann, B. Tillack, and K. Petermann, "Continuously tunable delay line based on SOI tapered Bragg gratings," Opt. Express 20, 11241 (2012).
11. Y. A. Vlasov, M. O'Boyle, H. F. Hamann, and S. J. McNab, "Active control of slow light on a chip with photonic crystal waveguides," Nature 438, 65–69 (2005).
12. D. O'Brien, A. Gomez-Iglesias, M. D. Settle, A. Michaeli, M. Salib, and T. F. Krauss, "Tunable optical delay using photonic crystal heterostructure nanocavities," Phys. Rev. B 76, 115110 (2007).
13. Joyce K. S. Poon, Jacob Scheuer, Yong Xu, and Amnon Yariv, "Designing coupled-resonator optical waveguide delay lines," J. Opt. Soc. Am. B 21, 1665-1673 (2004)
14. Sanghoon Chin, Luc Thévenaz, Juan Sancho, Salvador Sales, José Capmany, Perrine Berger, JérômeBourderionnet, and Daniel Dolfi, "Broadband true time delay for microwave signal processing, using slow light based on stimulated Brillouin scattering in optical fibers," Opt. Express 18, 22599-22613 (2010)15. D.
15. Marpaung, B. Morrison, M. Pagani, R. Pant, D.-Y. Choi, B. Luther-Davies, S. J. Madden, and B. J. Eggleton, "Low-power, chip-based stimulated Brillouin scattering microwave photonic filter with ultrahigh selectivity," Optica 2, 76 (2015).
16. Mégret, P. et al. "Ring resonator-based Tunable Optical Delay Line in LPCVD Waveguide Technology." (2005).
17. Guoliang Li, Jin Yao, Hiren Thacker, Attila Mekis, Xuezhe Zheng, Ivan Shubin, Ying Luo, Jin-hyoung Lee, Kannan Raj, John E. Cunningham, and Ashok V. Krishnamoorthy, "Ultralow-loss, high-density SOI optical waveguide routing for macrochip interconnects," Opt. Express 20, 12035-12039 (2012).
18. Lee, H., Chen, T., Li, J. et al. Ultra-low-loss optical delay line on a silicon chip. Nat Commun 3, 867 (2012). https://doi.org/10.1038/ncomms1876.
19. X. Ji, X. Yao, Y. Gan, A. Mohanty, M. A. Tadayon, C. P. Hendon, and M. Lipson, "On-chip tunable photonic delay line," APL Photonics 4(9), 090803 (2019).
20. Yariv, A., & Yeh, P. (2003). chapter 11. In Optical waves in crystals: Propagation and control of Laser Radiation (pp. 425–475). essay, John Wiley and Sons.
21. M. Heiblum and J. Harris, "Analysis of curved optical waveguides by conformal transformation," in IEEE Journal of Quantum Electronics, vol. 11, no. 2, pp. 75-83, February 1975, doi: 10.1109/JQE.1975.1068563.
22. Vaughan, John Michael. The Fabry–Perot interferometer: history, theory, practice and applications. Routledge, 2017.
23. N. Alshamrani, A. Grieco, B. Hong, and Y. Fainman, "Miniaturized integrated spectrometer using a silicon ring-grating design," Opt. Express 29(10), 15279–15287 (2021).
24. A. Grieco, B. Slutsky, D. T. H. Tan, S. Zamek, M. P. Nezhad, and Y. Fainman, "Optical bistability in a silicon waveguide distributed bragg reflector Fabry-pérot resonator," J. Lightwave Technol. 30(14), 2352–2355 (2012)
25. Appliednt.com. 2020. Nanosoi Fabrication Service | Applied NanotoolsInc.. [online] Available at: .https://www.appliednt.com/nanosoi-fabrication-service/
26. Appliednt.com. 2020. Nanosoi Fabrication Service | Applied NanotoolsInc.. [online] Available at: .https://www.appliednt.com/nanosoi/sys/resources/specs/.
27. Bykhovsky, D., Rosenblit, M., &Arnon, S. (2018). Two-sided through-wafer interconnect for optical spiral delay line. *Journal of Modern Optics*, *65*(1), 98–103. https://doi.org/10.1080/09500340.2017.1377305Y. Li, X. Song, Y. Xu, and Y. Li, "Spiral Optical Delay Lines in Silicon-on-Insulator," in Asia Communications and Photonics Conference 2016, OSA Technical Digest (online) (Optical Society of America, 2016), paper AF3G.6.
28. JingyaXie, Linjie Zhou, Zuxiang Li, Jinting Wang, and Jianping Chen, "Seven-bit reconfigurable optical true time delay line based on silicon integration," Opt. Express 22, 22707-22715 (2014)
29. Chen, T., Lee, H., &Vahala, K. J. (2014). Design and characterization of whispering-gallery spiral waveguides. *Optics Express*, *22*(5),5196. https://doi.org/10.1364/oe.22.005196
30. Yurtsever, G., Považay, B., Alex, A., Zabihian, B., Drexler, W., &Baets, R. (2014). Photonic integrated Mach-Zehnder interferometer with an on-chip reference arm for optical coherence tomography. *Biomedical Optics Express*, *5*(4), 1050.https://doi.org/10.1364/boe.5.001050.
31. Stopinski, S., Malinowski, M., Piramidowicz, R., Kleijn, E., Smit, M. K., &Leijtens, X. J. M. (2013). Integrated optical delay lines for time-division multiplexers. *IEEE Photonics Journal*, *5*(5).https://doi.org/10.1109/JPHOT.2013.2280519.